Available online at www.sciencedirect.com
SCIENCE DIRECT®
Pergamon
Acta Materialia 51 (2003) 1103–1113
Acta MATERIALIA
www.actamat-journals.com

Electrochemically-driven solid-state amorphization in lithium-silicon alloys and implications for lithium storage

Pimpa Limthongkul [a], Young-Il Jang [b], Nancy J. Dudney [b], Yet-Ming Chiang [a,*]

[a] *Department of Materials Science and Engineering, Massachusetts Institute of Technology, Cambridge, MA 02139, USA*
[b] *Condensed Matter Sciences Division, Oak Ridge National Laboratory, Oak Ridge, TN 37831, USA*

Received 24 June 2002; accepted 11 October 2002

Abstract

Lithiated metal alloys such as Li-Si are of great interest as high energy density anodes for future rechargeable battery technology. We show that the mechanism of electrochemical alloying is electrochemically-driven solid-state amorphization, a process closely analogous to the diffusive solid-state amorphization of thin films. X-ray diffraction and HREM experiments reveal that the crystallization of equilibrium intermetallic compounds is circumvented during lithiation at room temperature, and that formation of highly lithiated Li-Si glass instead occurs. This glass is shown to be metastable with respect to the equilibrium crystalline phases. Similar behavior is observed in the diffusive reaction of Li and Si bilayer films, suggesting that lithium-metal alloys in general are likely candidates for solid-state amorphization.

Keywords: Metallic glasses; Amorphous silicon; Thermodynamics; Phase transformation; Electrochemistry; Nanocrystalline materials

1. Introduction

Nearly 20 years ago, the formation of amorphous materials by a solid-state reaction rather than upon quenching from the melt, was observed in multilayered thin films [1]. The phenomenon is now known as solid-state amorphization (SSA). Solid-state amorphization occurs through diffusive reactions in multilayer films where the film thickness is comparable to interfacial thickness [1]. It has been explained as the formation of a glassy phase that is metastable, yet lower in free energy than the pure reactant phases, occurring when a thermodynamically preferred crystalline intermediate phase is unable to crystallize. SSA has similarities to earlier-observed reactive glass formation between bulk crystalline oxides such as SiO_2-Al_2O_3 [2]; both have been described in phase-diagram terms as metastable extensions of the liquidus curves to temperatures below the glass transition temperature (T_g) of the resulting liquid compositions. Reactions taking place below T_g, therefore, form a glass at rates determined primarily by solid-state interdiffusion [3].

Here we show that solid-state amorphization can be driven by electrochemical alloying. Using lith-

* Corresponding author. Tel.: +1-617-253-6471; fax: +1-617-253-6201.

1359-6454/03/$30.00
doi:10.1016/S1359-6454(02)00514-1

ium-silicon as a model system, this phenomenon, which we will refer to as *electrochemically-driven solid-state amorphization* (ESA), has been demonstrated using calibrated X-ray diffraction studies and high resolution electron microscopy of electrochemically lithiated alloys. There has been great recent interest in lithium storage at the negative electrode of rechargeable lithium batteries by alloying with Si or metals such as Al, Sn, and Sb, as alternatives to the intercalation of graphite. This is due to the intrinsically high gravimetric and volumetric energy densities possible by alloying [4–6], while having a lithium activity at the negative electrode that is sufficiently below that of pure Li metal to avoid dendrite formation and attendant safety problems in the presence of organic electrolytes. Silicon is of special interest since it has a maximum theoretical storage capacity for the $Li_{21}Si_5$ alloy of 4008 Ah/kg (9339 Ah/liter), more than tenfold greater than that of graphite, 372 Ah/kg (837 Ah/liter). The Achilles' heel of all such alloys has been the poor reversibility of the alloying process, attributed to mechanical failure [7] resulting from the large volume changes accompanying alloying. In order to cycle reversibly for durations practical in rechargeable battery systems, it has been suggested that synthesis of the metals in nanostructured form [8–10] is necessary. Recent studies in which nanoscopic Si [11,12] has been lithiated have resulted in disordered products, interpreted to be due to nanoscale size effects. Instead, we will demonstrate a common thermodynamic basis for the solid state amorphization of lithium-silicon alloys by electrochemical or conventional diffusive reactions, and show that it occurs in both bulk and thin film materials at room temperature. ESA should therefore be an important fundamental consideration in designing any electrochemical system operating near room temperature, including rechargeable lithium batteries of conventional or thin-film [13] design.

While to our knowledge thin-film solid-state amorphization has not previously been studied in any Li-Me alloy (Me is used hereafter to denote any of a number of metals such as Si, Sn, Al, Ag, Sb, and Zn), these alloys do exhibit many of the characteristics that are typically associated with metallic glasses formed by solid-state reaction, including: 1) negative heats of mixing; 2) large differences in atom size; 3) high alloying concentrations; and 4) large differences in the atom diffusivities [1,3,14–19]. These features favor mixing while also tending to yield a large nucleation barrier and instability of the daughter crystalline phase. The Li-Si phase diagram (Fig. 1 top) [20] exhibits numerous intermetallic phases, the nucleation and growth of which must be avoided if solid-state amorphization is to occur. The fact that the intermediate compounds have complex crystal structures [20] with little structural similarity to the pure endmembers was expected to help frustrate crystallization, since continuous transformation of, or epitaxial growth on, the parent phases is unlikely. Note that while electrochemical

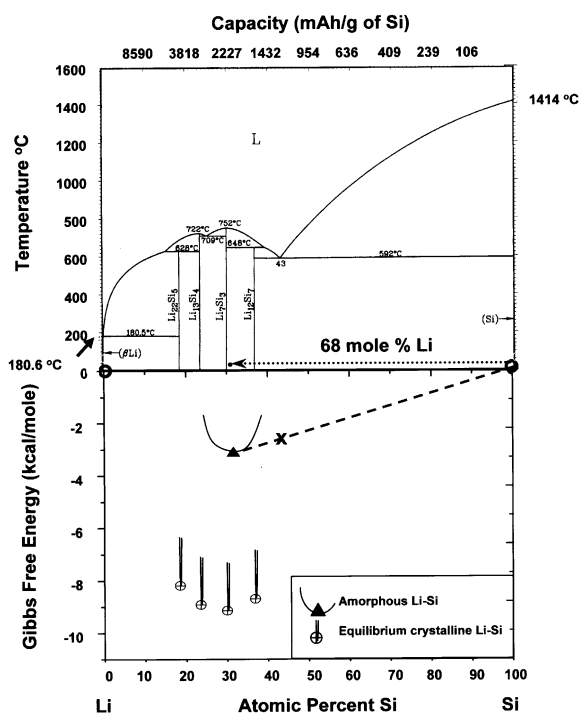

Fig. 1. (top) Equilibrium Li-Si phase diagram (ref. 14), and (bottom) Gibbs-free energy diagram for known crystalline phases and amorphous Li-Si alloy identified in this work. The overall composition of an electrochemically lithiated sample showing coexistence of crystalline Si and the metastable amorphous phase is denoted by X. When crystallization of the equilibrium intermetallic compounds is suppressed, electrochemically-driven solid state amorphization instead occurs at room temperature. See text for details.

measurements have been used to establish the phase relations in Li-Si as well as other Li-Me alloy systems, these have been conducted at elevated temperatures that promote the crystallization of the equilibrium intermetallic phases [21]. In this study, we carry out electrochemical alloying experiments at room temperature, where most battery systems are used and where crystallization of equilibrium phases is more readily avoided.

Fig. 2 illustrates the multiple possibilities that can occur when the lithium activity at a metal electrode is raised to values near unity using an electrochemical reaction. In case I, lithium metal may simply be electroplated, as is the case when alloying is thermodynamically prevented or if Li^+ is driven at too high a rate to allow reaction. In case II, electrochemically-driven supersaturation of the alloy might occur, if the electrode material can sustain an appreciable internal electric field. This situation is highly unlikely for the present conductive metal electrodes, although supersaturation may be possible in less conductive compounds such as the oxides. Case III is a conventional alloying situation in which the system forms solid solutions or crystalline compounds in accordance with the equilibrium phase diagram. This option is expected to occur at a rate limited by Li diffusion as in a binary diffusion couple. However, if the expected Li-Me crystalline phase formation is not kinetically permitted, but an amorphous phase formation with lower Gibbs energy than the reactants exists, case IV, solid-state amorphization, may instead occur.

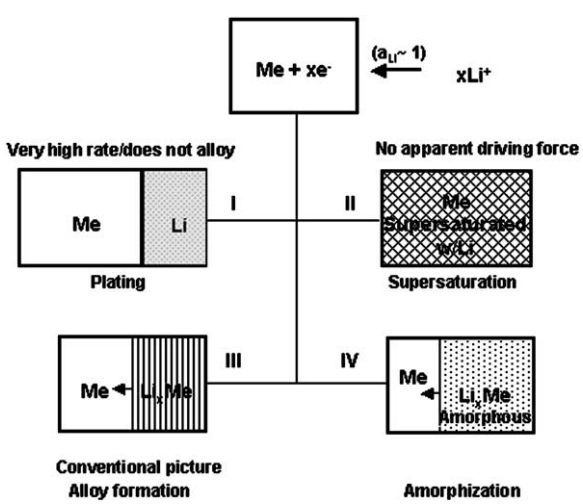

Fig. 2. Four different possibilities as a metal electrode is electrochemically lithiated: (I) Plating of Li metal on the surface, (II) Supersaturation of Li, (III) Equilibrium alloy formation, and (IV) Solid-state amorphization of the Li-metal alloy.

2. Experimental procedure

2.1. Electrochemical alloying and TEM

X-ray diffraction (XRD) and high resolution electron microscopy (HREM) experiments were performed on mixtures of electrochemically active Si (−325 mesh, 99.5% Alfa Aesar, Ward Hill, MA) mixed with a non-reactive internal standard of fine nickel powder (0.08–0.15 μm, 99.8% Alfa Aesar). This simple measure allowed the amount of crystalline silicon phase present throughout the electrochemically-induced transformation to be quantified. (It is possible that solid-state amorphization has been overlooked in previous studies due to the absence of internal standards.) Electrodes were prepared by mixing the Si and Ni powders with polyvinylidene fluoride binder, PVDF (534,000 MW, Aldrich, Allentown, PA) in a 6:3:1 weight ratio, using γ-butyrolactone (99+%, Aldrich) as the solvent, in an Ar-filled glovebox with less than 3 ppm oxygen and H_2O. The powder/binder mixture was dried, pressed into $^1/_4''$ diameter pellets of ~100 μm thickness, and assembled in a standard stainless steel electrochemical cell with Teflon™ insulator. The pellets were tested as the positive electrode against Li foil (0.75 mm thick, Alfa Aesar) as the negative electrode, using Celgard 2400™ (Celgard Inc., Charlotte, NC) as the polymer film separator. The electrolyte used was a 1 M solution of $LiPF_6$ in a 1:1 mixture (by weight) of ethylene carbonate, EC, and dimethyl carbonate, DMC (EM Science, Norwood, OH). The electrochemical tests were carried out at room temperature at a constant current density of 10 mA/g of active metal.

X-ray diffraction was performed before and after lithiation of the sample, using a Rigaku diffractometer (Rigaku, RU300, continuous scan with 0.75° scan speed, 0.02° interval, 1° divergence and scatter slits and 0.3° receiving slit with Cu-Kα

radiation). The highly reactive lithiated samples were handled in an Ar-filled glovebox to prevent oxidation, and the metal powder was extracted from the electrochemical cells and mounted on a glass slide using Kapton™ tape (VWR Scientific, West Chester, PA) to prevent reaction with the ambient atmosphere during XRD. The starting mixture served as a reference standard of known Si/Ni fraction, from which the relative amounts of crystalline phases after lithiation were quantified [22].

High resolution and analytical electron microscopy experiments were performed using a JEOL 2010FX TEM (JEOL, Ltd., Tokyo, Japan) operating at 200 keV and equipped with an energy-dispersive X-ray detector (Link Systems, Oxford Instrument, High Wycombe, UK). The lithiated positive electrodes were prepared for electron microscopy by ultrasonically dispersing a small piece of the pellet in γ-butyrolactone (99+%, Aldrich), and placing the suspension on a nickel or copper grid coated with a carbon film or lacey carbon coated formvar film (EM Microscopy Science, Fort Washington, PA). All handling of the sample, as well as loading of the sample into the TEM specimen holder, was conducted in the Ar-filled glovebox. The specimen holder was transported in a sealed container, and loaded into the TEM with less than 30 s exposure to air.

2.2. Thin-film diffusive reactions

To make a direct comparison of the electrochemically alloyed samples to the same reactants in a conventional thin film geometry, Si films of 0.5 μm thickness were deposited on polycrystalline Al_2O_3 plates by dc magnetron sputtering of a Si target (99.999%, Kurt J. Lesker) in Ar atmosphere. The films were annealed at 1000 °C for 10 h in Ar to insure crystallinity. Li films of 1.5 μm were then deposited on the Si films by thermal vapor deposition of Li metal at temperature ~50–80 °C, to obtain a bilayer with overall Li/Si molar ratio of 2.82.

The bilayer films were packaged under a layer of lithium phosphorous oxynitride (Lipon) [23] of 0.2 μm thickness, deposited by rf magnetron sputtering of Li_3PO_4 in N_2 atmosphere. Between the Li and Lipon depositions, the samples were handled in an Ar-filled glove box.

3. Results and discussion

3.1. Electrochemical and microstructural characterization

When a Si powder sample is lithiated to a total charge capacity of 1280 mAh/g (Li/Si molar ratio of 1.34, or 57 mole% Li), the voltage profile, Fig. 3 solid line, shows a flat voltage plateau at 0.1V that suggests a two-phase field of constant lithium chemical potential. In this dynamic measurement, the observed voltage can include various polarizations and cannot be taken as the equilibrium voltage. The equilibrium voltage over this composition range was measured by interrupting this test at 200 mAh/g capacity intervals and holding for 4 h, whereupon the cell voltage relaxes to a steady-state value. This voltage profile and the measured equilibrium open-circuit voltage is shown in Fig. 3. With increasing lithiation, a constant equilibrium

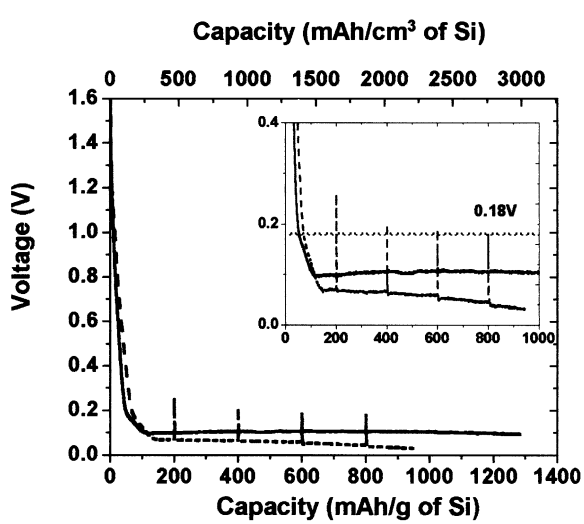

Fig. 3. Voltage vs storage capacity profiles for lithiation of crystalline Si. Solid line shows sample continuously lithiated to 1280 mAh/g (1.34 mole Li/mole of total Si, 57 mole% Li/total Si). Dashed line shows interrupted test whereby cell voltage is allowed to relax to the equilibrium voltage. The equilibrium voltage appears at a lower voltage than expected for equilibrium $Li_{12}Si_7$–Si coexistence (0.34 V).

voltage of 0.18 V is reached. If coexistence of the equilibrium crystalline phases Si and $Li_{12}Si_7$ were to occur, the results of Wen and Huggins [24] show that an equilibrium voltage of ~0.34 V with respect to pure Li metal would be expected. The lower equilibrium voltage we see indicates a significant deviation from equilibrium.

Fig. 4a and b compare X-ray diffractograms of the Ni and Si powder mixture before and after lithiation. If equilibrium were maintained along this composition trajectory, $Li_{12}Si_7$ should crystallize and increase in relative fraction while coexisting with crystalline Si. Fig. 4c does show a decrease in the Si phase reflections relative to the Ni reference, from which it was determined that 38 mole% of the starting silicon phase remained. However, no new reflections showing formation of any crystalline phase appeared. From the remaining crystalline Si fraction and the total lithium transported (Fig. 3), the average Li/Si molar ratio of the reaction product was calculated to be 2.17 (68 mole% Li, or a composition $LiSi_{0.47}$). This composition is shown as the terminal composition along the trajectory in Fig. 1, and lies clearly within the equilibrium $Li_{12}Si_7$–Si two-phase field.

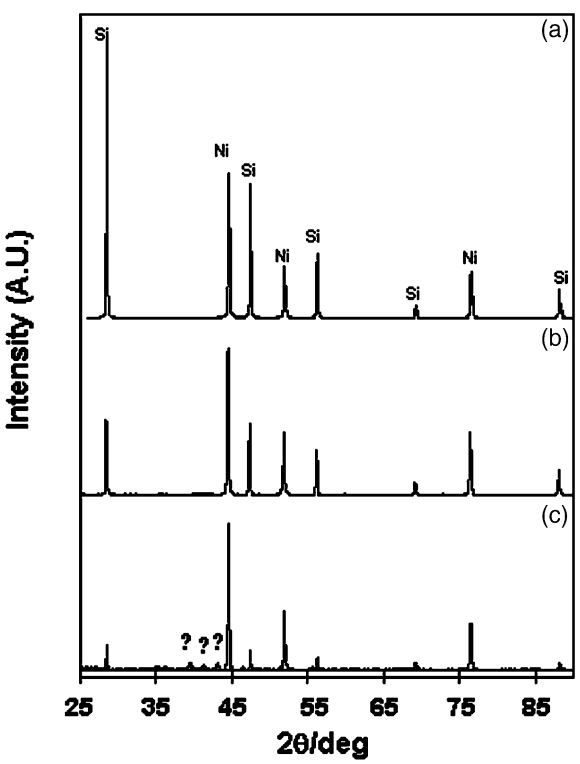

Fig. 4. X-ray diffraction experiment using Ni as an internal standard to calibrate the fraction of remaining crystalline Si upon electrochemical lithiation. a) the starting mixture of Si:Ni:PVDF (60:30:10 weight ratio), b) Si sample lithiated to 57 mole% Li/total Si, and c) Si sample lithiated to 69 mole% Li/total Si. No new crystalline phases accompany the decrease in Si fraction in b). In c), none of the three Li-Si intermediate phases expected to form in sequence could be detected, but unidentified broad peaks appeared at $2\theta = 39.4°$, 41.3° and 43.1° suggesting a metastable ordered phase.

High resolution and analytical electron microscopy showed that the sample was found to be dominated by amorphous phase particles, the composition of which was found via energy-dispersive X-ray analysis (EDX) to be Si-rich. Fig. 5 shows the HREM bright field images, corresponding dark field images, a typical selected-area diffraction pattern, and an energy-dispersive spectrum typical of the amorphous phase particles. The bright-field images showed a periodic contrast with no lattice fringes or changes in diffraction contrast upon tilting. The electron diffraction patterns showed diffuse rings characteristic of a glass. The dark field images formed using the diffracted intensity from the first diffuse ring, as in Fig. 5b,

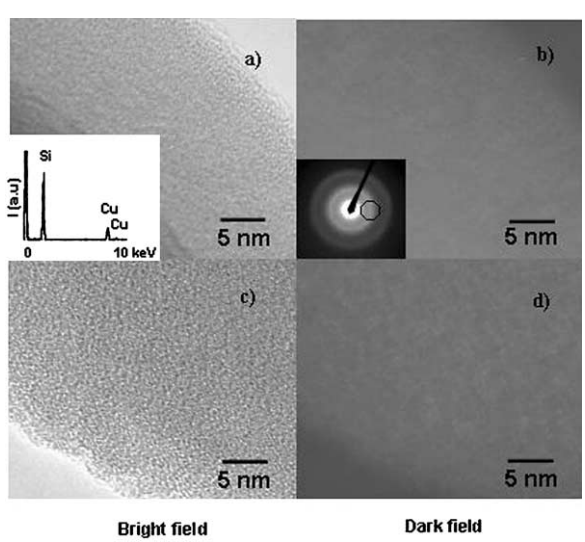

Fig. 5. HREM bright field images (a,c) and their corresponding dark field images (b,d) showing microstructure of Si after lithiation to 68 mole% Li, showing that electrochemical lithiation has resulted in production of an amorphous alloy.

showed homogeneous scattering intensity and no sign of strongly diffracting regions larger than a few angstroms, confirming the absence of crystalline phases. The EDX spectrum showed predominantly Si. While Li is not detectable with the detector used, the low oxygen concentration in these amorphous phase particles is important since they rule out the two most likely artifacts possible in this experiment. The low oxygen content shows that the particles are neither oxidized amorphous silicon oxide formed during inadvertent exposure of the highly reactive lithiated alloy to air, nor the product of a reaction between the alloy and the organic liquid electrolyte (known as the solid-electrolyte interface, or SEI), which are typically a mixture of organic species and metal carbonates. The majority of the particles analyzed by HREM were of this type. SEI layers were occasionally observed, and were readily identified by the strong oxygen line observed in the EDX spectrum, in contrast to the spectra in Figs. 5 and 7. Some crystalline Si particles were also observed, consistent with the XRD results. In some cases the coexistence of amorphous phase with a central core of crystalline Si were observed in the same particle. Thus, the physical coexistence of an amorphous phase and crystalline silicon was confirmed, consistent with the constant lithium chemical potential implied by the voltage plateau in Fig. 3.

The structural characteristics of this ESA product can be compared to that of amorphous Si produced by vapor-deposition and annealing, in the classical study by Moss et al. [25]. We analyzed the scattered intensity in the electron diffraction patterns taken from various lithiated silicon particles as a function of scattering vector, *k*, using SEMPER™ software (Synoptics Ltd., Cambridge, UK). Results from four such patterns are plotted in Fig. 6, where they can be compared against those from a vapor-deposited amorphous Si film [25]. Within the experimental error, determined primarily by the contrast in the diffraction pattern and the spatial resolution of the analysis software, the analyzed intensities can be seen to be very similar to those from the amorphous Si film, having broad peaks at *k*-vector ~2.0 $Å^{-1}$ and at ~3.6 $Å^{-1}$.

Since the scattered intensity is proportional to the square of atomic scattering factor [22], the contribution of Li atoms is in this case more than an order of magnitude less than that of Si. The scattered intensity from the lithiated sample can be primarily attributed to the Si substructure within the amorphous alloy. The close correspondence of diffraction peaks in Fig. 6 indicates similar atomic arrangements in the lithiated Si to that of the conventional amorphous Si. The atomic arrangement in conventional amorphous Si has long been considered to be the exemplar of a continuous-random network glass [26]. The present data, therefore, suggest that the structure of amorphous Li-Si produced by electrochemical lithiation consists of a

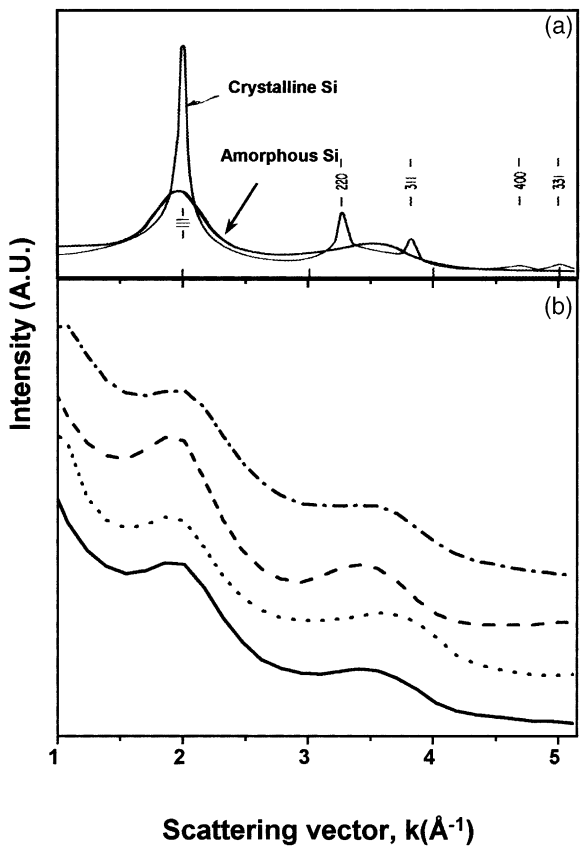

Fig. 6. Comparison of the scattered electron intensity profile as a function of scattering vector (*k*-vector) in: a) vapor-deposited amorphous Si film before and after crystallization (ref. 25), and b) a Si sample electrochemically lithiated to 68 mole% Li in this work. The similarities suggest a continuous random network silicon substructure for the lithiated alloy.

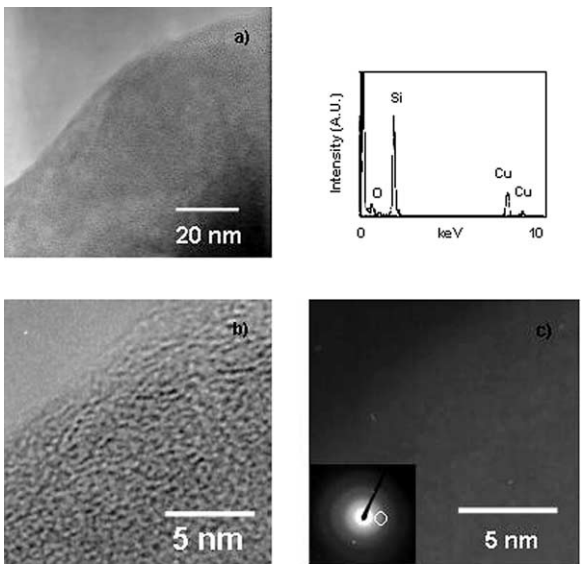

Fig. 7. HREM bright field image a) at low magnification, b) at high magnification, and c) a corresponding dark field image of (b), of Si lithiated to a higher concentration of 74 mole% Li, falling within the Li_7Si_3 and $Li_{13}Si_4$ equilibrium two-phase field. The lithiated composition instead consists predominantly of a Si based amorphous phase.

continuous-random network of Si tetrahedra, into the interstices of which Li atoms are inserted. This structure differs significantly from that of the expected crystalline phase, $Li_{12}Si_7$ [27] in which planar Si_5 rings are accompanied by planar Si_4 stars and Li atoms to form an extended orthorhombic crystal structure.

3.2. Thermodynamic interpretation

As the experimental data has shown, the Li-Si system follows the fourth option in Fig. 2 and forms an amorphous Li-Si phase upon electrochemical lithiation. Standard free energies of formation are available for the pure metals as well as the equilibrium crystalline intermetallic compounds in Fig. 1, here listed in Table 1 [28,29]. Combined with the electrochemical test data, we construct in Fig. 1 (bottom) a Gibbs free energy diagram for all presently known crystalline phases in this system and the amorphous phase of this work. The standard Gibbs free energy of pure Li and Si are shown for the experimental temperature

Table 1
Standard Gibbs free energies of for Li at 25 °C [28], Si at 25 °C [28] and Li-Si Alloys at 415 °C [29], and amorphous Li-Si alloy at 25 °C from the present work

Phases	G_i (kcal/mole)
Li	−2.072
$Li_{12}Si_7$	−199.516
Li_7Si_3	−109.944
$Li_{13}Si_4$	−183.956
$Li_{22}Si_5$	−273.375
amorphous $LiSi_{0.47}$ (This work)	−4.151
Si	−1.341

of 293 K (± 3 K). The equilibrium Li-Si crystalline phases are treated as line compounds, consistent with the phase diagram (Fig. 1). Although experimental thermodynamic data are only available for these compounds at a temperature of 688 K (415 °C), the formation free energies are likely to vary by less than 1% between 688 K and room temperature. For the amorphous phase, the composition was assumed to be $LiSi_{0.47}$, as determined from the diffraction analysis and electrochemical test. Its free energy was determined using the Nernst equation, $\Delta G^o_{LiSi_{0.47}} = -nFV = -4.15$ kcal/mole, where V is the experimental equilibrium voltage of the amorphous alloy with respect to pure lithium, F is Faraday's constant, and *n*, the number of electrons transported per Li^+, is unity.

The free energy construction (Fig. 1) is consistent in every aspect with the experimental observations. The crystalline intermetallics do have much lower Gibbs energy than the amorphous alloy, but clearly do not easily crystallize at room temperature, in contrast to the behavior observed under the elevated temperature conditions of ref. 29. As the silicon is lithiated, crystalline Si and the amorphous Li-Si phase of approximately constant composition coexist, consistent with the long voltage plateau observed in the electrochemical test. The XRD results confirm that the only crystalline phase present (aside from the nonreactive internal standard) is Si, and the HREM results show only crystalline Si and the amorphous Si-containing phase. The coexistence of an SSA-produced amorphous phase and a crystalline phase has pre-

viously been observed in thin film reactions, one example being the Au-La thin film system [1].

3.3. Amorphous and metastable ordered phases forming at higher lithiation

Another experiment was conducted in which three crystalline Li-Si phases would have been expected to form sequentially if equilibrium was maintained. A Si sample was electrochemically lithiated to a higher capacity of 2170 mAh/g, corresponding to a Li/Si molar ratio of 2.26 or 69 mole% Li. The voltage profile (not shown) was similar to that in Fig. 3, exhibiting a nearly flat voltage plateau ending at 0.09 V. Fig. 4c shows the X-ray diffractogram after lithiation. The remaining crystalline Si, calculated from the decrease in the integrated peak intensities for the Si phase reflections relative to those for the Ni reference, was 10 mole% of the starting silicon in this case. The electrochemically lithiated fraction was calculated by difference to have an average Li/Si molar ratio of 2.82 (74 mole% of Li), which falls within the Li_7Si_3 and $Li_{13}Si_4$ coexistence field in Fig. 1. It can be seen that if equilibrium were maintained, upon lithiation the $Li_{12}Si_7$ phase would first form and then disappear, being replaced by the crystalline phases Li_7Si_3 and $Li_{13}Si_4$ as the terminal composition is approached. As in the earlier sample, XRD showed that none of the expected crystalline intermetallic compounds form. However, small unidentified broad peaks at $2\theta = 39.4°$, 41.3° and 43.1°, corresponding to *d*-spacings of 2.3 Å, 2.2 Å, and 2.1 Å, were detected. These peaks do not correspond to any of the Li_7Si_3 and Si peaks, nor do the relative intensities of these peaks match those of equilibrium Li-Si compounds [30].

HREM showed that this sample also consists primarily of amorphous phase particles (Fig. 7), with electron diffraction showing diffuse rings at the same position as in the previous sample (Fig. 5). However, the sample also showed the presence of nanoscale ordered regions (Fig. 8). The composition of these particles was found by energy-dispersive X-ray analysis (EDX) to also be Si-rich, but the structure could not be conclusively identified. The XRD and HREM results suggest that at higher Li concentration, the amorphous Li-Si alloy begins to form an ordered phase that is also metastable, and is structurally distinct from any of the equilibrium crystalline phases.

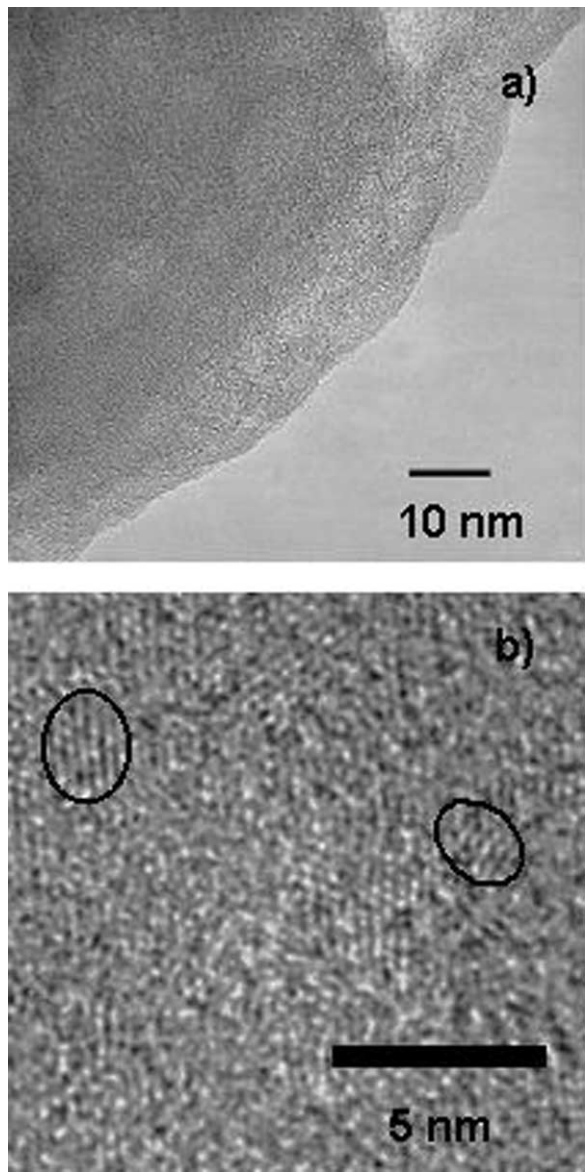

Fig. 8. Within certain particles in the sample lithiated to a higher concentration of 74 mole% Li, here viewed at low and high magnification, nanoscale ordered regions are evident.

3.4. Thin-film solid-state amorphization in Li-Si

Thin film bilayer experiments showed that in this system, solid-state reaction between Li and Si thin films occurs readily at 50–80 °C. The overall Li/Si molar ratio of this diffusion couple is 2.82, close to that of the electrochemically alloyed sample discussed above. XRD results of the Si film before deposition, and after Li film deposition are shown in Fig. 9. A reduction in Si integrated peak intensity of about a factor of 4 is observed. However, as in the electrochemical lithiation experiments, no peaks were found that could be associated with any of the equilibrium Li-Si crystalline phases. Minor peaks from unidentified phase(s) are seen in Fig. 9. These peaks, which were not seen in the electrochemically alloyed samples, could correspond to a Li-Si metastable phase that formed due to a higher reaction temperature during Li deposition (~50–80 °C). The majority reaction product appears to be amorphous. It is not surprising that Li-Si thin films react readily at temperatures below 80 °C, given the rapid Li transport rate at room temperature (necessary for these alloys to function electrochemically at room temperature). In related work, we have seen rapid reaction at the same temperature range in Li-Sn thin film couples as well. Electron microscopy was not accomplished on these samples due to the difficulty of preparing electron-transparent foils of highly lithiated alloys without oxidation. The results nonetheless demonstrate, as we hypothesized, the close analogy between ESA and conventional thin-film SSA reactions.

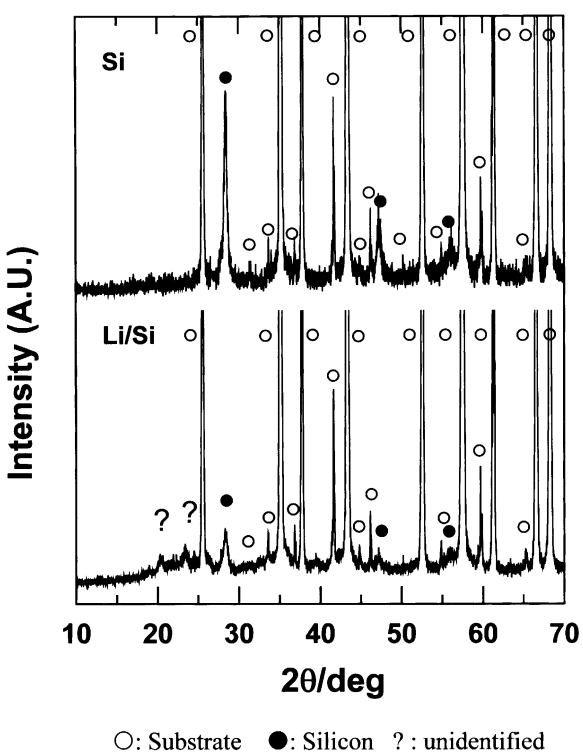

Fig. 9. X-ray diffraction from the thin film solid-state reaction of Li with Si at a molar ratio of 2.82 Li/Si (74 mole% Li). Diffractogram of starting Si film is shown at top. The substrate is Al_2O_3. At bottom, results from the Li/Si bilayer formed thermal evaporation of Li at 50–80 °C onto the Si film showed that none of the expected equilibrium crystalline Li-Si compounds associated with this overall composition are observed.

3.5. Other lithiated alloy systems

We now comment briefly on experiments in other Li-Me systems which support the model of ESA. These results will be published elsewhere. In the Li-Sn system, it was found that none of the equilibrium Li-Sn crystalline phases formed upon room temperature electrochemical lithiation of powders or thin-film solid-state reaction. A metastable disordered reaction product showing weak broad diffraction peaks, similar to that reported by Dahn et al. [31] was observed. In the Li-Ag system, fine (0.1 μm) Ag powders formed a substantial amount of crystalline LiAg upon lithiation. However, using internal standards in XRD, we found that the crystalline LiAg and α-Ag solid solution together comprise only one-half of the total Ag present. This implies that the remainder is present as amorphous Li-Ag alloy, consistent with HREM observations showing an amorphous phase. Furthermore, the crystalline LiAg fraction increased significantly in lithiated samples during several days of room temperature storage, indicating the crystallization of this amorphous Li-Ag alloy over time. In Li-Al, we appear to have found a system that does not easily undergo electrochemically-driven solid-state amorphization. Calibrated XRD showed that lithiation of fine powders at room temperature resulted in nearly complete

LiAl formation, which may be due to easy nucleation of its simple NaTl structure type [32].

4. Conclusions

The microscopic reaction mechanism occurring when metals are electrochemically lithiated at room temperature has been studied. In the system Li-Si, experiments have been conducted which demonstrate the phenomenon of electrochemically-driven solid-state amorphization, in which a metastable Li-Si glass is formed when the crystallization of equilibrium intermediate compounds is frustrated. Li-Si bilayer thin films are similarly found to react without forming any of the expected equilibrium crystalline phases, suggesting that Li-Me alloys in general are likely candidates for solid state amorphization. A self-consistent thermodynamic interpretation was obtained in the Li-Si system. Nanoscale size effects are not necessary for this phenomenon to take place; crystallization is readily avoided in Li-Si at room temperature. Combined with similar initial results in Li-Ag and Li-Sn, we suggest that this concept may occur widely in lithiated alloys that are of interest for electrochemical energy storage, and should be taken into account in the design of storage alloys and their microstructures.

Acknowledgements

The authors thank W. Craig Carter and John B. Vander Sande for helpful discussions. Funding and instrumentation in the Shared Experimental Facilities at MIT were supported by NSF grant no. 9400334-DMR. Support for Y.I.J. and N.J.D. was provided by the US Department of Energy's Division of Materials Sciences and Division of Chemical Sciences under contract DE-AC05-00OR22725 with the Oak Ridge National Laboratory, managed by UT-Battelle, LLC.

References

[1] Schwarz RB, Johnson WL. Phys Rev Lett 1983;51:415.
[2] Aksay IA, Pask JA. J Am Ceram Soc 1975;58:507.
[3] Johnson WL. Amorphization by interfacial reactions. In: Yip S, editor. Materials interfaces: atomic-level structure and properties. 1st ed. New York: Chapman & Hall; 1992. p. 51-6.
[4] Yao NP, Heredy LA, Saunders RC. J Electrochem Soc 1971;118:1039.
[5] Besenhard JO, Yang J, Winter M. Journal of Power Sources 1997;68:87.
[6] Lai SC. J Electrochem Soc 1976;123:1196.
[7] Huggins RA, Nix WD. Ionics 2000;6:57.
[8] Turner RL, Mcclure DJ, Buckett MI, Dahn JR, Mao O. International Patent WO, 99/49532, 2000.
[9] Mao O, Turner RL, Courtney IA, Fredericksen BD, Buckett MI, Krause LJ et al. Electrochem Solid Stat Lett 1999;2:3.
[10] Yang J, Winter M, Besenhard JO. Solid State Ionics 1996;90:281.
[11] Zhou GW, Li H, Sun HP, Yu DP, Wang YQ, Huang XJ et al. Appl Phys Lett 1999;75:2447.
[12] Gao B, Sinha S, Fleming L, Zhou O. Adv Mater 2001;13:816.
[13] Bates JB, Dudney NJ, Neudecken BJ, Wang B. Energy storage systems in electronics. In: Datta M, editor. New trends in electrochemical technology. Lamghorne, PA: Gordon and Breach; 1998. p. 453.
[14] Anantharaman TR. Metallic glasses: production properties and applications. Aedermannsdorf, Switzerland: Trans Tech Publications, 1984 p. ii, 305.
[15] Lin C, Yang GW, Liu BX. Phys Rev B 2000;61:15649.
[16] Egami T. J Non-Cryst Solids 1996;207:575.
[17] Egami T. Materials Science and Engineering. Structural Materials Properties Microstructure and Processing 1997;226:261.
[18] Chen HS, Jackson KA. The Influence of Alloy Composition on Glass Formation and Properties. In: Metallic glasses: papers presented at a seminar of the Materials Science Division of the American Society for Metals, September 18 and 19, 1976. Metals Park, OH: American Society for Metals, 1978. p. 74.
[19] Polk DE, Giessen BC. Overview of Principle and Applications. In: Metallic glasses: papers presented at a seminar of the Materials Science Division of the American Society for Metals, September 18 and 19, 1976. Metals Park, OH: American Society for Metals, 1978. p. 1.
[20] Okamoto H. In: Massalski TB, editor. Binary alloy phase diagram, 1. Materials Park, OH: ASM International; 1990.
[21] Boukamp BA, Lesh GC, Huggins RA. J Electrochem Soc 1981;128:725.
[22] Cullity BD. Elements of X-Ray Diffraction, 2nd ed. Reading, MA: Addison-Wesley Pub. Co, 1978 p. 397.
[23] Yu X, Bates JB, Jellison Jr GE, Hart FX. J Electrochem Soc 1997;144:524.
[24] Wen CJ, Huggins RA. J Solid Stat Chem 1981;37:271.
[25] Moss SC, Graczyk JF. Phys Rev Lett 1969;23:1167.
[26] Polk DE. J Non-Cryst Solids 1971;5:365.
[27] von Schenering HG, Nesper R, Curda J, Tebbe KF. Angew Chem Int Ed 1980;19:1033.

[28] Barin I, Platzki G. Thermochemical data of pure substances, 3rd ed. New York: VCH: Weinheim, 1995.
[29] Anani AA, Huggins RA. J Electrochem Soc 1987;134:C407.
[30] JCPDS card number 40-0942, 29-0830, 18-0747, 27-1402-International Centre for Diffraction Data.
[31] Dahn JR, Courtney IA, Mao O. Solid State Ionics 1998;111:289.
[32] McAlister AJ. In: Massalski TB, editor. Binary alloy phase diagram, 1. Materials Park, OH: ASM International; 1990. p. 167